Park et al. *NPG Asia Materials* (2022) 14:40
https://doi.org/10.1038/s41427-022-00386-4

NPG Asia Materials

ARTICLE Open Access

Individually addressable and flexible pressure sensor matrixes with ZnO nanotube arrays on graphene

Junbeom Park[1], Ramesh Ghosh[1,2], Minho S. Song[1,3], Yunjae Hwang[1], Youngbin Tchoe[4], Rajendra Kumar Saroj[1], Asad Ali[1], Puspendu Guha[1,3], Bosung Kim[5], Sang-Woo Kim[5], Miyoung Kim[6] and Gyu-Chul Yi[1,3]

Abstract

We report the fabrication of individually addressable, high-density, vertical zinc oxide (ZnO) nanotube pressure sensor arrays. High-sensitivity and flexible piezoelectric sensors were fabricated using dimension- and position-controlled, vertical, and free-standing ZnO nanotubes on a graphene substrate. Significant pressure/force responses were achieved from small devices composed of only single, 3 × 3, 5 × 5, and 250 × 250 ZnO nanotube arrays on graphene. An individually addressable pixel matrix was fabricated by arranging the top and bottom electrodes of the sensors in a crossbar configuration. We investigated the uniformity and robustness of pressure/force spatial mapping by considering the pixel size, the number of ZnO nanotubes in each pixel, and the lateral dimensions of individual ZnO nanotubes. A spatial resolution as high as 1058 dpi was achieved for a Schottky diode-based force/pressure sensor composed of ZnO nanotubes on a flexible substrate. Additionally, we confirmed the excellent flexibility and electrical robustness of the free-standing sensor arrays for high-resolution tactile imaging. We believe that this work opens important opportunities for 1D piezoelectric pressure/force sensor arrays with enormous applications in human-electronics interfaces, smart skin, and micro- and nanoelectromechanical systems.

Introduction

One-dimensional (1D) piezoelectric semiconductor nanostructures, including nanowires, nanotubes, and nanorods, have demonstrated enormous application opportunities in nanoelectromechanical energy harvesters, consumer electronics, robotics, and health care sectors[1–12]. The 1D nanowires/nanotubes can be assembled and vertically arranged within a tiny area to serve as a pressure/force sensor array with high spatial resolution arising from mapping of pressure/force with considerably high sensitivity. Among a variety of wurtzite-structured piezoelectric semiconductor materials, such as zinc oxide (ZnO), gallium nitride (GaN), aluminum nitride (AlN), and zinc sulfide (ZnS), 1D ZnO nanostructures have attracted tremendous attention; furthermore, they are widely used as sensing platforms for artificial intelligence and medical devices by coupling piezoelectricity with photonics and electronics[1,8]. In recent years, significant effort has been devoted to studying superior nanomaterials and subsequent nano/microfabrication of tactile sensors for applications in flexible electronics. A functional tactile sensing device for next-generation robotics and human–machine interfaces requires large-scale integration of pressure sensor arrays with high spatial resolution, high sensitivity, wide detection range, fast response, and good substrate flexibility[6,13–19].

A variety of flexible and stretchable tactile sensors with different pressure sensing mechanisms have been studied, including resistive, capacitive, triboelectric, and piezoelectric

Correspondence: Ramesh Ghosh (Ramesh.Ghosh@glasgow.ac.uk) or Gyu-Chul Yi (gcyi@snu.ac.kr)
[1]Department of Physics and Astronomy & Institute of Applied Physics, Seoul National University, Seoul 08826, Republic of Korea
[2]James Watt School of Engineering, University of Glasgow, Glasgow G12 8QQ, UK
Full list of author information is available at the end of the article
These authors contributed equally: Junbeom Park, Ramesh Ghosh.

types[6,13–25]. The active materials of resistive tactile sensors are conductive nanomaterials in a polymer matrix. Although there are some advantages for resistive tactile sensors, such as high sensitivity with controlled spatial resolution, simple device structure, and cost-effective fabrication, the application range is narrow because of existing drawbacks, such as high power consumption and temperature dependence of the devices[13,19–21]. Capacitive tactile sensors are the most common sensors and have demonstrated low power consumption, significant flexibility, reliable device performance over a wide range of pressures, high sensitivity and considerable spatial resolution[13,14,22–24]. Bulk device structures, inconsistent device performance depending on the dielectric elastomers, complex measurement processes, and limited spatial resolution are the main drawbacks for utilizing capacitive tactile sensors in high-resolution pressure/force mapping[13,14,22–24]. Because of their self-powered and energy harvesting features, triboelectric tactile sensors have attracted enormous attention from researchers. High sensitivity for detection of pressure from diverse types of forces has been demonstrated by measuring the differences in triboelectric polarities for the two contacting materials. Dynamic pressure sensing has been regarded as a challenge for triboelectric tactile sensors[8,13,14]. Piezoelectric tactile sensors are widely studied because of their promising performance, such as high sensitivity, fast response, and ability to sense dynamic pressures[8,13,14,16]. Among different piezoelectric materials and different types of nanostructures, 1D ZnO nanostructures on flexible substrates have attracted tremendous attention in efforts to overcome the drawbacks remaining in the field of tactile image sensors[2,8,13,16].

Researchers have adopted different approaches to achieve outstanding performance from piezoelectric ZnO-based tactile sensors by forming heterostructures and composites as well as integrating photonics with piezotronics[2,10,13,15,26–28]. Piezo-phototronic sensors have demonstrated enormous spatial resolution, rapid response time, and device flexibility[2,10,13,26–28]. Liu et al. reported high-spatial resolution piezotronic tactile sensors based on 2D ZnO nanoplatelets[15]. Integration of the 1D ZnO nanostructures on a flexible substrate as independently addressable and piezotronic sensor arrays for high-resolution (>1000 dpi) pressure/force mapping is still limited by the technically challenging fabrication process. This requires significant research on developing high-density integrated 1D nanostructure-based piezoelectronic devices to address the challenges associated with this field. Enormous control of dimension and position is essential for synthesizing good-quality, high-density 1D ZnO nanostructures and for controlled fabrication of sensor device arrays. It has proven to be extremely challenging to fabricate high-density, individually operated two- or three-terminal device arrays using vertical 1D nanostructures[29]. Therefore, a two-terminal crossbar electrode array was established to fabricate high-density, individually addressable device arrays to avoid extreme device complexity[12,29]. An important approach is to flip the 1D nanostructures to construct crossbar electrode arrays on the two ends of 1D nanostructure arrays[12,29–31]. Metal-organic chemical vapor deposition (MOCVD) is a well-established method for fabricating high-quality, dimensional, and position-controlled 1D ZnO nanotube (NT) arrays on graphene films[29–32]. The bottom graphene layer controls the dimension and positions of ZnO NTs and provides effective lift-off of the free-standing ZnO NTs to form efficient crossbar microelectrodes[29–32]. More importantly, these discrete 1D nanostructures integrated on elastic substrates constitute excellent material platforms for flexible tactile devices in e-skin. Graphene films exhibit excellent mechanical stability for bending and twisting; therefore, they are used directly as a flexible conductive layer for improving the robustness of the contacts[29,32,33].

In this work, we fabricated individually addressable, flexible, free-standing vertical 1D nanostructure pressure/force sensor arrays using high-quality ZnO nanotube arrays on graphene films. Catalyst-free metal-organic vapor phase epitaxial (MOVPE) growth of ZnO NTs was performed directly on graphene film with high crystallinity and precisely controlled dimensions and positions. The graphene film enabled easy lift-off of the 1D ZnO NTs from the substrate to form efficient crossbar electrodes and achieve flexible and reliable free-standing sensor arrays. Individual devices consisting of a single nanotube and small 3×3 and 5×5 bundles of nanotubes within an area $\leq 20 \times 20\ \mu m^2$ showed excellent piezoelectric responses to very small pressures imparted by the flow of inert gas. High sensitivity, fast response, and a wide detection range have been achieved from each of these different types of sensors. An 8×8 matrix of individually addressable sensors was fabricated and examined to demonstrate a proof-of-concept pixel-addressable matrix. Furthermore, we investigated the uniformity and robustness for spatial mapping of pressure/force by considering the pixel size, the number of ZnO nanotubes in each pixel, and the lateral dimensions of individual ZnO nanotubes. A spatial resolution as high as 1058 dpi was achieved from a Schottky diode comprising ZnO nanotubes on a flexible substrate. Overall, the work reported here represents a significant step toward next-generation tactile sensors broadly applicable for wearable electronics, consumer electronics, robotics, and health care.

Materials and methods

Growth of ZnO nanotube arrays on graphene layers

Chemical vapor deposition (CVD) growth and transfer of the graphene layers

Large-area, multilayered graphene films were synthesized on Cu foil (0.025 mm thick; 99.8% (metal basis);

Alfa Aesar) by using the CVD method. First, the Cu foil was cleaned with acetone (J.T. Baker) and isopropanol (IPA) (J.T. Baker) and inserted into a tubular quartz tube. After that, the chamber was heated to 1030 °C with a continuous H_2 (>99.9999%) flow of 100 SCCM at 200 Torr. After reaching 1030 °C, the Cu foil was annealed for 15 min to coarsen the grain while maintaining the flow rate and reactor pressure. Graphene films were then grown on the Cu foil for 130 min under a mixture of CH_4 (>99.999%) and H_2 at flow rates of 10 and 100 sccm, respectively. Furthermore, the reactor pressure was maintained at 220 Torr during growth. Finally, the sample was cooled to room temperature under a H_2 atmosphere while keeping the chamber pressure at 200 Torr. After synthesizing thin graphene layers on the Cu foil, the polymethyl methacrylate (PMMA; Microchem) layer was spin-coated on the top surface of the Cu foil, while the graphene film synthesized on the backside of the Cu foil was removed by oxygen plasma ashing (SPI Plasma Prep II). The Cu foil dissolved completely once the sample was immersed in an ammonium persulfate solution, leaving only the PMMA-supported graphene layers on the surface of the solution. Finally, the PMMA-supported graphene films were transferred onto a SiO_2-coated Si substrate (300 nm wet-oxidized, p-type boron-doped Si wafer; thickness: 675 ± 25 μm; resistivity: 1–30 -cm; University Wafer), and the PMMA layer was removed using organic solvents.

Substrate preparation for ZnO NT growth

A thin SiO_2 layer with a thickness of 50 nm was created on the as-transferred CVD-graphene layer by using a commercial plasma-enhanced CVD system. The oxide layer was annealed at 600 °C in O_2 (>99.9999%) before the patterning process to reduce the number of defects in the as-deposited SiO_2 film that would otherwise cause undesired growth and reduce growth selectivity. Thereafter, hole patterns on the growth mask were defined by electron beam lithography. After lithography, the SiO_2 film was dry-etched using CF_4 plasma (RIE; Oxford Plasmalab 80), followed by wet etching using buffered oxide etchant (BOE; J.T. Baker). The residual oxide layer remaining on the graphene after dry etching was removed entirely using BOE. After that, the substrates were cleaned in acetone and 2-propanol, followed by nitric acid, and finally rinsed in DI water to obtain the array pattern on graphene.

MOVPE growth of the ZnO nanotube array on graphene layers

Position-controlled ZnO nanotube arrays were grown on graphene films using MOVPE with a homemade MOCVD system[29,31]. The ZnO nanotubes were grown on predefined areas that were created by electron beam lithography patterning and intended etching of the growth mask. Diethylzinc (DEZn) (>99.999%; EPICHEM) and high-purity O_2 were used as reactants, and high-purity Ar (>99.9999%) was used as the carrier gas. The flow rates of DEZn and O_2 were 40 and 100 SCCM, respectively. During growth, Ar flowed into the quartz reactor through the bubbler with a bubbler temperature of −10 °C maintained by DEZn. The O_2 gas line was separated from the main gas manifold line to prevent premature reaction. The reactor pressure was kept at 3.2 Torr, while the temperature was fixed at 690 °C during growth.

Lift-off process for free-standing ZnO nanotubes on graphene

After preparing the ZnO nanotube arrays on CVD graphene layers, a polyimide (PI) layer (VTEC™ PI) was formed on the sample by spin coating at 4000 rpm. After that, the PI layer was prebaked at 120 °C for 120 s to evaporate all solvents. The PI layer was mostly formed on the bottom side of the ZnO nanotubes with a thin coating on the tips of the nanotubes. The ZnO nanotubes were then exposed to oxygen plasma treatment (Plasma Prep II) for 5 min at 50 mA under 50 mTorr to selectively etch the PI layers at the tip. Thereafter, the entire layer was mechanically lifted from the substrate by separating the graphene film from the loosely bonded SiO_2 substrate with the aid of a Kapton tape frame. The PI layer supported the ZnO NTs to be suspended in free-standing conditions, and the bottom ends of the ZnO NTs were free for contact deposition. The free-standing PI layer composed of ZnO nanotube/graphene layers was cured under a N_2 (>99.9999%) atmosphere in a homemade rapid thermal annealing (RTA) system using two-step curing (at 200 °C for 3 min and at 300 °C for 3 min)[29,32].

Fabrication methods for individually addressable nanotube device arrays

Top and bottom electrode lines were formed by transferring the layer onto the polished surface of a highly doped n-type Si substrate for electron-beam lithography (EBL). Biolayer e-beam resist layers (PMMA 950 K/495 K) were used to promote easy lift-off of the metal leads. Top Au electrode lines were then formed on the ZnO nanotube array by using standard EBL, 100-nm-thick Au deposition, and subsequent metal lift-off procedures. We used the grazing angle metal deposition method to conformally coat Au electrodes onto the ZnO nanotube surface. A metal flux incident angle of 20° with respect to the normal axis of the substrate was used while rotating the substrate at 1 rpm. In this configuration, a thin Au layer was conformally deposited on the upright sidewalls of the ZnO nanotubes after depositing a 100-nm-thick Au layer on the PI surface. After that, the free-standing layer was flipped and transferred onto an *n*-Si substrate to

create Cr/Au (10/100 nm) bottom electrodes on the graphene layers in the same manner. The unprotected graphene layer on the backside was etched using oxygen plasma, leaving the back electrodes underneath graphene strips. Crossbar electrode arrays were obtained to provide a matrix of 8 × 8 devices. We used two different widths for the crossbar electrode channels to integrate different amounts of nanotubes. For example, electrodes with 12 μm and 20 μm widths and the same periodicity were used for 3 × 3 and 5 × 5 arrays of ZnO nanotubes, respectively. Organization of cross-bar array (8 × 8) electrodes across the ZnO nanotubes made 8 × 8 crosses for the addressable devices. Each crossing point was termed a "dot". A pixel in the addressable devices was defined by the periodicity of the respective device arrays[12,34]. The addressable device with a pixel area of 24 × 24 μm^2 (dot size of 12 μm) was termed AD12, while it was named AD20 for a 40 × 40 μm^2 pixel area (dot size of 20 μm). The spatial resolution of the respective devices was defined in standard dots per inch (dpi) units. Two-terminal individual sensors were also fabricated in which only single ZnO, 3 × 3, 5 × 5, and 250 × 250 NTs were integrated.

Characterization of nanotube device arrays

Morphology and structural characterization

The morphologies of the ZnO nanotube arrays were investigated with a field-emission scanning electron microscope (FESEM, TESCAN) operated at 30 kV. Morphology analyses of the microdevices at different stages of fabrication were performed by normal SEM (AURIGA; Carl Zeiss). This system was used for e-beam lithography to control the dimension and spacing of ZnO NT growth on graphene. Furthermore, the same system was used to design the crossbar electrode arrays used to fabricate the addressable matrix arrays. Individual ZnO NTs and their crystal lattice fringes were studied with a field-emission transmission electron microscope (analytical TEM, JEM-2100F, JEOL Ltd.). For this analysis, the ZnO NTs were scratched and dispersed in isopropanol and later drop-cast onto a lacey-carbon-coated Cu TEM grid (300 mesh; Tedpella).

Electrical characterization

The sensing capabilities of the prototype sensors were characterized by measuring current-voltage (I-V) and current-time (IT) curves during the presence/absence of pressure on the sensor. A constant DC bias voltage was applied to the device during the pressure/force sensing performance via the source meter (Keithley-2601).

Measurement of pressure/force sensing characteristics

The pressure sensing characteristics, i.e., the piezoresistive properties of the ZnO nanotubes, were investigated by examining current responses under the impulse of constant mechanical pressure. Specifically, a mechanical force in the range 0.1–1 kg-wt in intervals of 0.1 kg-wt was applied to the sensor. Sensors were firmly attached to a flat surface to subject one surface to a vertical force. Notably, a flat and polished sapphire substrate (1 mm^2) was placed between the force applying tip and the sensor to avoid formation of unwanted electrical pathways.

A constant flow of inert gas (argon), monitored by a mass flow controller (MFC), was used to investigate the response for a small pressure. The constant flow of inert gas imparted uniform and constant pressure on the sensor. The pressure sensor device was placed on a solid substance at a distance of 2 mm from the output of the MFC. The pressure/force response was investigated with different Ar flow rates in SCCM units.

The individual pressure responses of the free-standing, flexible sensor arrays were measured in a probe station by connecting the counter electrodes with two Au probes. Pressure/force was applied in two different ways. An additional probe was used, which was controlled by a high-precision knob, to apply mechanical pressure. However, a small pressure was applied by a contactless argon flow monitored by the MFC. The constant flow of argon was directed at an angle of 45° with the surface of the device.

Results and discussion

Fabrication and structures of the sensors

High-quality ZnO nanotube arrays were hetero-epitaxially grown on chemical vapor-deposited (CVD) graphene layers using selective-area metal-organic vapor phase epitaxy (MOVPE) to fabricate 1D semiconductor nanostructure-based pressure/force sensors. The positions and dimensions of the vertical ZnO nanotube samples were controlled by changing the lithography design and growth parameters. Figure 1a, b shows the top-view and 30° tilted-view scanning electron microscopy (SEM) images of ZnO NT arrays on graphene, respectively. Figure 1c shows an enlarged view of an individual ZnO NT. The diameter and length of the ZnO NTs were found to be 500 nm and 9–10 μm, respectively. The steps involved in the growth of dimension- and position-controlled ZnO NTs on graphene are schematically shown in Fig. S1a–d. Figure 1d, e shows top-view and 30° tilted-view SEM images of ZnO NT-based sensor arrays on graphene, respectively. Figure 1f shows an enlarged view of an individual sensor. The steps involved in fabricating the sensors are shown schematically in Fig. S1e–i. The outer wall of the ZnO NT was interconnected by ultrathin ZnO walls. Figure S2a–f shows SEM images of six different ZnO NTs; the images confirm the formation of interconnected ultrathin walls inside the hollow NTs in each case. The average wall thickness of the ZnO NTs was

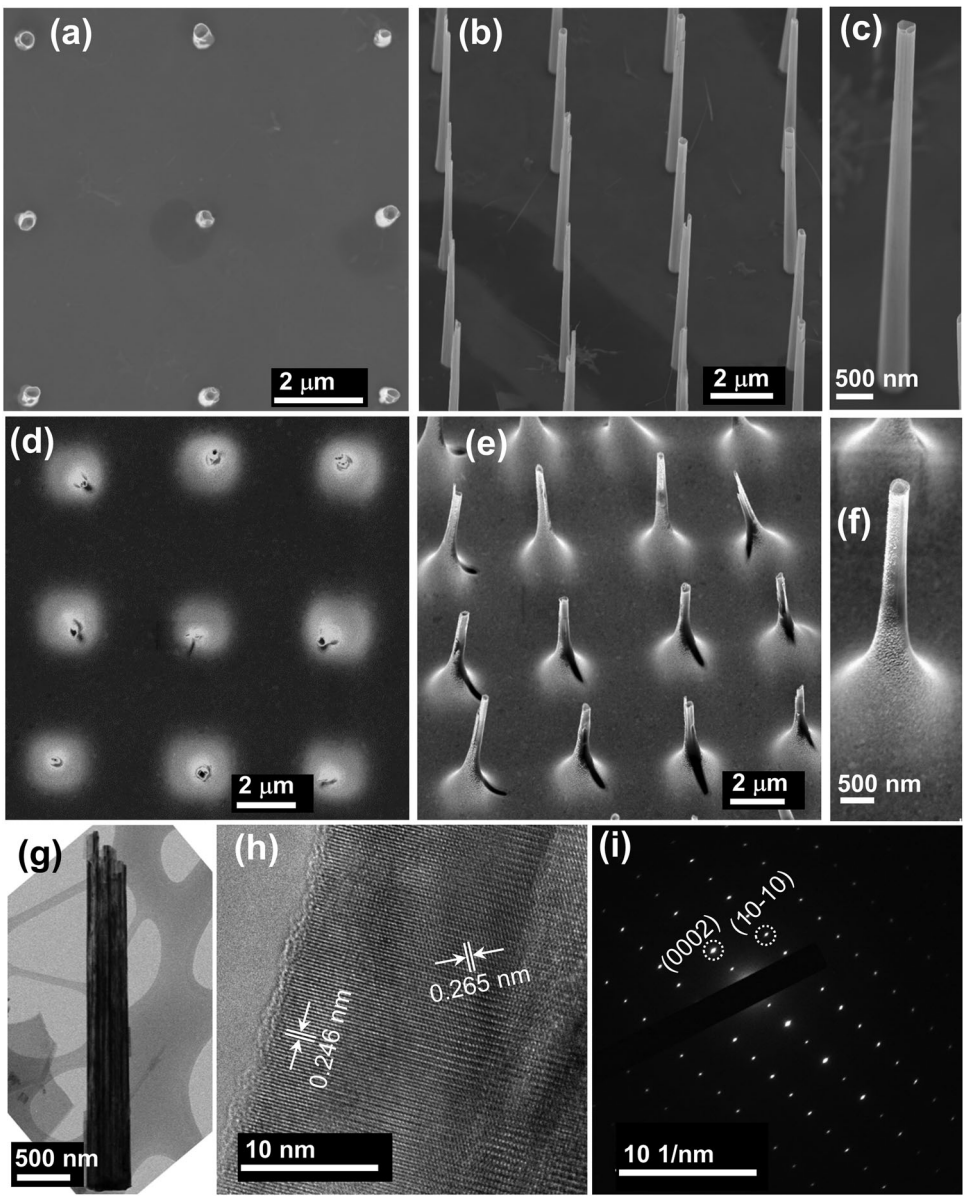

Fig. 1 Morphology of ZnO NT-based pressure sensor. a Top-view and **b** 30° tilted-view SEM images of ZnO NT arrays on graphene. **c** SEM images of a single ZnO NT with 30° tilted views. **d** Top-view and **e** 30° tilted-view SEM images of ZnO NT-based pressure sensor arrays on graphene. **f** 30° tilted-view SEM images of a single ZnO NT-based pressure sensor. **g** TEM image of an individual ZnO NT collected after scratching the ZnO NTs on a Cu grid. **h**, **i** Corresponding HRTEM lattice image and SAED pattern, respectively.

found to be 12 nm. The bright-field transmission electron microscopy (TEM) image in Fig. 1g further confirmed the formation of interconnected ZnO nanowalls inside the hollow nanotube. These structures prevent the NTs from breaking the sensors under excessive pressure. Furthermore, the high-resolution TEM image and selected area diffraction pattern in Fig. 1h, i confirmed the high crystallinity of ZnO and its suitability for piezoelectric applications. SEM images of the free-standing sensor device (see Fig. 1d–f and Fig. S2g–l) confirmed that gold was coated conformally on the ZnO NTs. The average sidewall thickness of gold was found to be 17 nm toward the top of the ZnO NTs. Fig. S1j shows the schematic cross-section of a device and indicates each layer. The device structure consisted of a Schottky contact at the top end of the ZnO NTs (ZnO-Au), while an ohmic contact was placed at the NT bottom side (ZnO-graphene-Cr-Au)[29,32]. Ultrasmall samples were grown containing only single NTs as well as 9 and 25 NTs in addition to bulk production of ZnO NT arrays (2500 NTs) on graphene.

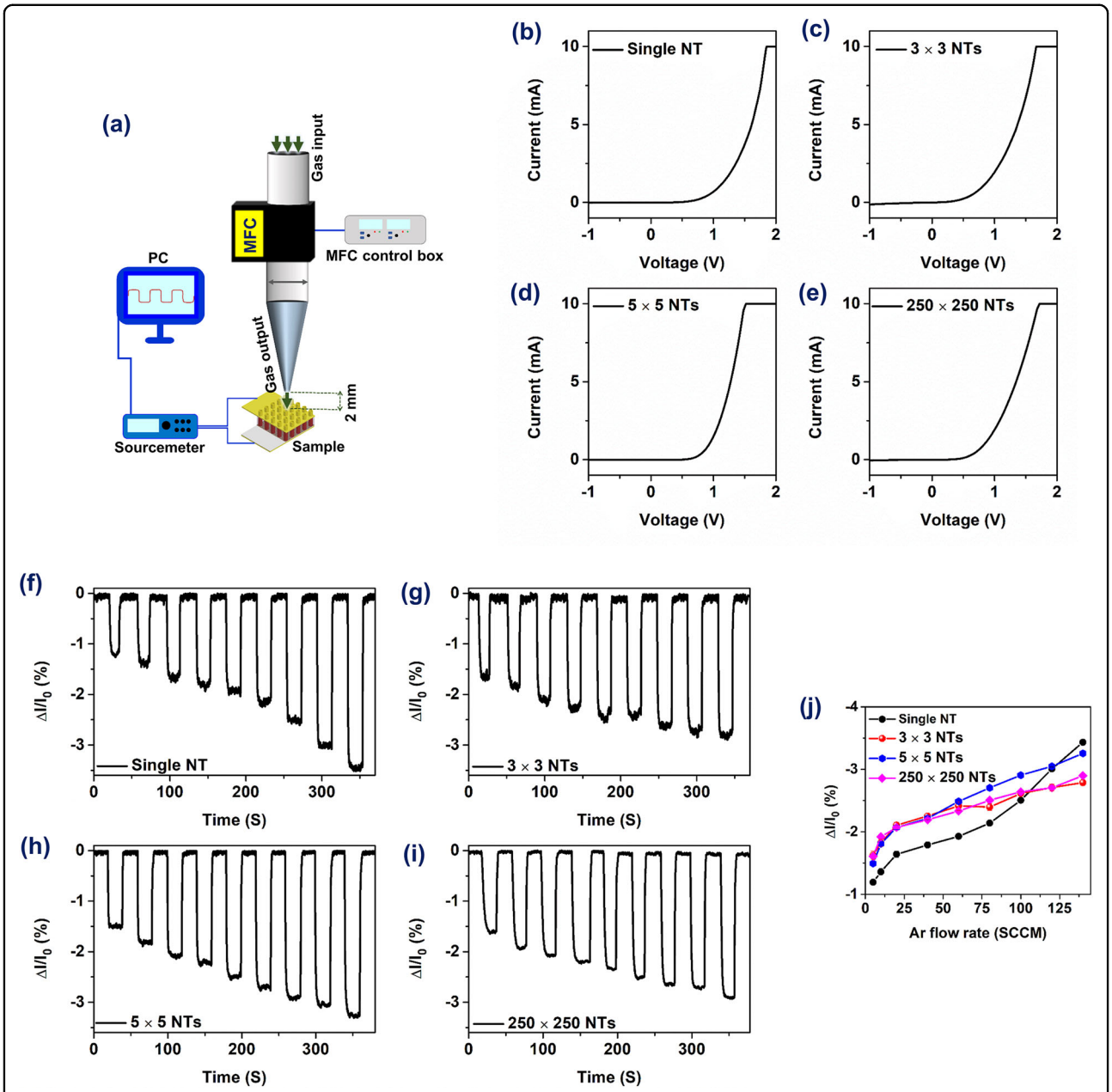

Fig. 2 Pressure responses of the sensors. a Schematic representation of the experimental setup used to measure pressure responses when pressure was imparted by a constant flow of inert gas. **b**–**e** *I*–*V* characteristics of pressure sensors containing single, 3 × 3, 5 × 5, and 250 × 250 NTs, respectively. **f**–**i** Corresponding real-time pressure responses with different argon gas flow rates ranging from 5 to 140 SCCM. **j** Comparison of the response as a function of argon flow rate from pressure sensors containing different ZnO NTs.

Figure S3a–c shows a schematic representation of the ZnO nanotubes on graphene samples containing single NT, 3 × 3, and 5 × 5 NTs, respectively, while Fig. S3d–f shows their corresponding SEM images. The diameter and length (or their averages when multiple NTs were involved) of the ZnO NTs were found to be 500 nm and 9–10 μm, respectively, whereas the periodicity was 4 μm. A schematic illustration and corresponding SEM images of different NT-containing samples after PI coating are shown in Fig. S3g–l. Furthermore, a schematic representation and corresponding SEM images of the fabricated devices are shown in Fig. S3m–r.

Pressure detection characteristics of the nanotube devices

We investigated the electrical characteristics of nanotube device arrays under normal and strained conditions. The experimental setup used for applying pressure on the sample is shown schematically in Fig. 2a.

The current–voltage (I–V) characteristics of the single, 3 × 3, 5 × 5, and 250 × 250 NT-based sensors are shown in Fig. 2b–e. Each curve indicated that the sensors were Schottky diode-type; hence, they exhibited mostly rectifying behavior. The Au-ZnO junction was Schottky-type, whereas the ZnO-graphene-Cr-Au showed an ohmic nature[29,32]. The I–V characteristics in Fig. 2b–e revealed that there were barrier heights for these devices, indicating a turn-on voltage in the forward bias; hence, the current was very low with a very low forward bias voltage[29,35]. The pressure/force responses of the devices were measured via changes in current levels under a constant bias voltage, which was higher than the turn-on voltage for the device. The pressure/force responses of the devices were measured by calculating the current varying ratios, $\Delta I/I_0$. Therefore, we investigated the pressure/force responses of the devices by subjecting them to constant pressure/force with a constant flow of inert gas (argon). Figure 2f–i shows the real-time pressure/force response as a function of SCCM for the devices containing single, 3 × 3, 5 × 5, and 250 × 250 NTs, respectively. The pressure sensing mechanism is shown schematically in Fig. S4. With the application of pressure, the strain-induced electrons moved to the interface between Au and ZnO. Enrichment of electrons at the interface led to an increased Schottky barrier height (Fig. S4d). As a result, the current through the sensor was decreased. Note that a systematic increase in response was observed from each device when the pressure applied to the devices was increased gradually. Figure 2j compares the responses as a function of argon flow rate from pressure sensors with different ZnO NTs. Fluctuation in pressure response were low for devices in which multiple NTs were involved. However, each device could detect a small pressure imparted from a low flow rate of 5 SCCM. Figure 2j indicates that the response curves for single NT and 5 × 5 NT-based sensors were slightly steeper than those of the 3 × 3 and 250 × 250 NT-based sensors. The pressure responses of the sensors depended on the morphologies of the individual ZnO NTs, especially in cases with single or few NT-based sensors. Additionally, the direction of gas flow caused a small difference in the effective pressure applied on the vertically aligned and slightly slanted ZnO NTs. These might be reasons for the small discrepancies in the response curves in Fig. 2j. On the other hand, the turn-on voltages for these 4 different devices were slightly different, as shown in Fig. 2b–e, which could also have an effect on the responsive nature of the 4 devices. In a typical case, these were similar for 3 × 3 and 250 × 250 NT-based sensors (Fig. 2c, e), confirming the similar response behaviors shown in Figure (j). Note that the overall nature of the response curves in Fig. 2j for the 4 devices were similar. This further motivated us to fabricate high-resolution addressable pressure sensors in which each pixel would comprise only a few ZnO NTs. Furthermore, a large-area device was used with 250 × 250 NTs within an effective device size of 1 mm^2 to investigate the sensitivity. The force was applied on the sensor with a 1 mm sapphire stamp within the range 0.1–1.0 kg-wt with regular increases of 0.1 kg-wt. Figure S5a shows the real-time responses for different applied forces. Estimates of the pressure responses of the sensor are presented in Fig. S5b; the sensitivity was found to be 1.95 ± 0.06 MPa^{-1}. We observed that the ZnO NTs in the sensors were broken at high pressure[32]. Note that the interconnected walls inside the hollow ZnO NT partially protected them from breaking when large forces were applied. A 20 μm thick polymer (PMMA) was used as a protecting layer on the sensors to enable estimating the sensitivity and the detection range of the sensors. Fig. S6 shows a comparison of the pressure responses from the 4 different types of PMMA-coated sensors for different mechanical pressures. The sensitivities of the devices were found to be 0.55 ± 0.04 MPa^{-1}, 0.54 ± 0.02 MPa^{-1}, 0.43 ± 0.06 MPa^{-1}, 0.88 ± 0.06 MPa^{-1} for the pressure sensors containing single, 3 × 3, 5 × 5, and 250 × 250 NTs, respectively. The sensitivities of the devices decreased drastically after PMMA coating. Therefore, the actual sensitivities of the single, 3 × 3, 5 × 5, and 250 × 250 NT-based sensors were much higher than the measured values. It is interesting to see that a 20 μm PMMA layer could increase device stability even after applying a very high pressure (3000 kPa). Eventually, the devices exhibited compromises in sensitivity as well as in device performance. Fig. S6 shows that the pressure responses for the single ZnO NT-based sensors were saturated when the pressure was ~1600 kPa, while saturation in pressure responses occurred over ~1900 kPa for the rest of the devices. The as-prepared sensors were suitable for detecting low pressures, while the sensors with a protecting layer were suitable for sensing extremely high pressures. The response times were also measured for the as-prepared sensors. Fig. S7 compares the response times of the 4 devices. In each case, the response time was relatively small (<100 mS), which indicated that the prototypes could be suitable for high-frequency sweeping. Support of the free-standing sensors by polyimide made them flexible; therefore, they can be transferred to any foreign substrate. Notably, the electrical characteristics of the devices were unaltered upon considerable bending of the substrate[32]. The high sensitivity, ability to detect ultralow pressures, wide detection range, fast response time, and small yet robust structures motivate us to fabricate small area, pixel-addressable, flexible, and wearable sensor arrays from vertically aligned ZnO NT arrays on graphene.

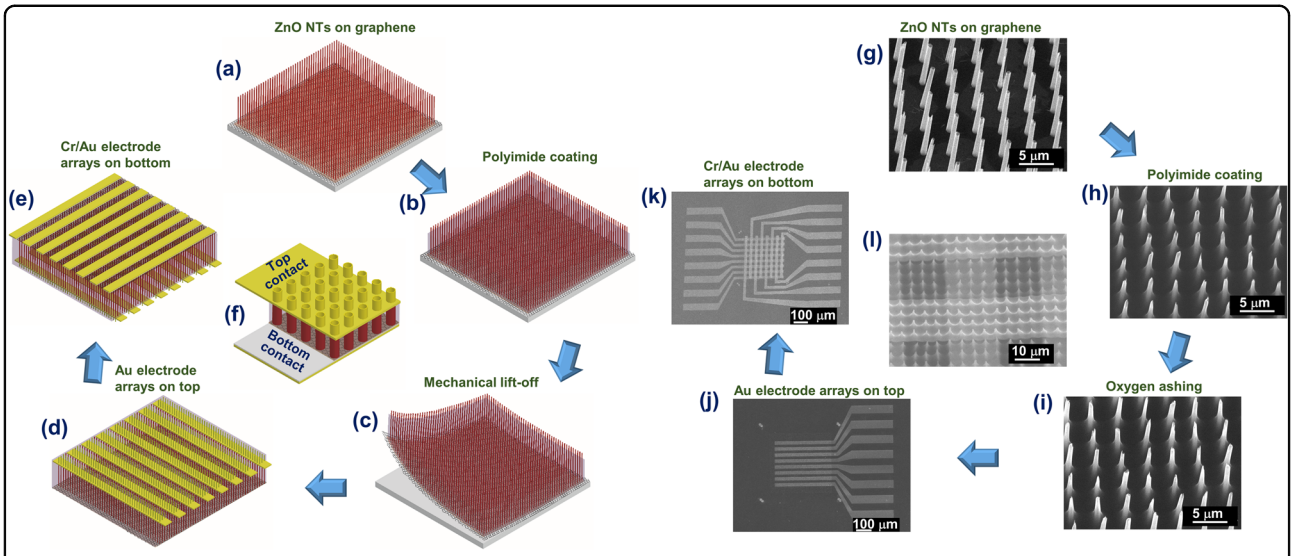

Fig. 3 Fabrication of addressable sensor arrays. a–e Schematic illustration of the steps used to fabricate crossbar array electrodes. **f** Enlarged view of the addressable device AD20. **g–k** SEM images at different stages of AD20 fabrication. **l** SEM image of a complete, individually addressable device. SEM images in **g–l**, **i**, and **l** are tilted by 30°.

Fabrication of addressable devices

The process flow was identical to the individual device fabrication method for fabrication of free-standing, addressable sensor arrays. Additional lithography was used to define the electrode arrays on the top and bottom ends of the ZnO NTs. The step-by-step process for preparation of an 8 × 8 matrix for the device is shown schematically in Fig. 3a–e along with a single pixel in Fig. 3f containing 5 × 5 ZnO NTs. SEM images captured at different stages of the fabrication process for device AD20 are also shown in Fig. 3g–k. A magnified SEM view of the completed device is shown in Fig. 3l. Figure S8 shows SEM images of devices AD20 and AD12 containing 8 × 8 crossbar matrixes on ZnO NTs with different pixel dimensions. Note that the addressable sensor arrays were fabricated using ZnO NTs with tube diameters of both 500 nm and 1 μm and fixed heights of 9 μm. The devices were finally attached to a printed circuit board (PCB) frame for electrical characterization.

Spatial mapping of pressure from the addressable devices

The $I–V$ and $I–T$ characteristics of the 8 × 8 sensor matrix array were investigated to obtain a spatial map of pressure. The pressure was imparted by a uniform flow of argon gas (monitored by MFC) through a pipette tube of 2 mm diameter, which was kept 2 mm from the sample and at an angle of 45° with the sample plane. Figure 4a shows a schematic representation of the measurement setup (upper panel) and the corresponding digital photograph (bottom panel). Figure 4b, c shows the $I–V$ data for different pixels from two different samples, AD12 and AD20. The individual sensors in each pixel of a sample showed different barrier heights and different turn-on voltages. The observed nonuniformity of the individual nanotube devices presumably resulted from the nanotube geometry, which was composed of 29-nm-thick nanowalls[29].

The pressure responses of individual sensors in each pixel were investigated at a fixed bias of 1.5 V and at a constant pressure by feeding Ar gas with a uniform flow rate of 140 SCCM. Figure 3d, e shows the real-time responses of different pixels from two different samples, AD12 and AD20. Figure 4f, g shows the corresponding spatial map of the pressure response. Each pixel of the two different samples responded efficiently to pressure, although variations in responses were obtained. The average pressure response was found to be 1.38 ± 0.25% for AD12; however, it was 1.47 ± 0.31% for AD20. The observed irregularity in the pressure responses from the individual nanotube devices was likely due to nonuniformity in the Schottky barriers of different pixels. Nanoscale variations in the morphologies of nanotubes resulted in different metal-semiconductor interfacial areas. This may also have an effect on the individual responses of the different pixels. Additionally, the Schottky barrier height is strongly influenced by the size of the diode because the contribution of tunneling to the total conductance is significantly enhanced for small diodes[36]. In this study, a Au/ZnO Schottky junction was formed on the sharp tip of the NT wall and was expected to have a small barrier height. Hence, the effective barrier heights of the addressable devices were different, which resulted in inconsistency in the pressure response. Note that inhomogeneities in the Au layer thickness along the

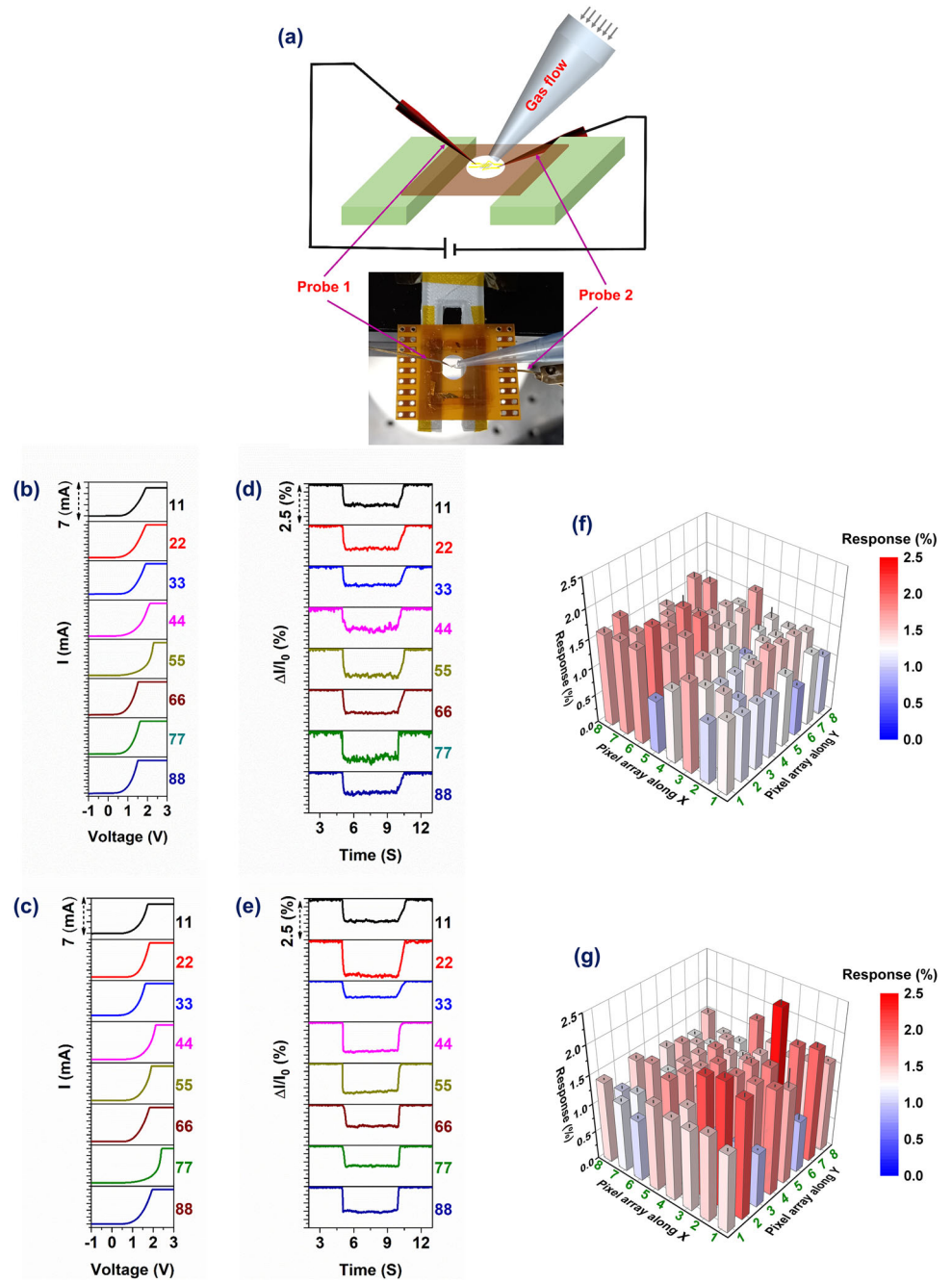

Fig. 4 Spatial distribution of the pressure responses during uniform flow of inert gas. a Schematic illustration of the experimental setup (upper panel) used to detect inert gas pressure. Corresponding digital photograph (bottom panel). Comparison of *I*–*V* plots from eight diagonal pixels in the devices **b** AD12 and **c** AD20. Comparison of the real-time responses from eight diagonal pixels with an argon flow rate of 140 SCCM in the devices **d** AD12 and **e** AD12. Spatial distributions of pressure responses at an argon flow rate of 140 SCCM from addressable devices **f** AD12 and **g** AD12.

circumferential direction of the ZnO NTs can also produce strain, which might also be partially responsible for the nonuniform pressure responses of the addressable devices.

The same AD20 was fabricated, which was composed of ZnO NT arrays with a diameter of 1 μm, to reduce the effect of the sharp tip size and small contact area on the response characteristics. Figure S9a, b shows the real-time responses of different pixels and a spatial map of the pressure response. The average pressure response was found to be 1.43 ± 0.17%, and this was relatively small compared to the response variations

Table 1 Summary of addressable pressure sensors and their performance parameters.

Material system	Device type	Sensitivity (KPa^{-1})	Sensing method	Spatial resolution (dpi)	Reference
ZnO NW/GaN	LED	12.88×10^{-6}	Piezo-phototronic	6350	[26]
ZnO-nanofilm/Si-micropillar	LED		Piezo-phototronic	4885	[27]
ZnO-nanofilm/PDMS/Si-microwire	LED		Piezo-phototronic	4300	[28]
ZnO NW/PEDOT:PSS	LED		Piezo-phototronic	3628	[2]
GaN/ZnO NW	LED		Piezo-phototronic	9769	[10]
ZnO thin film	Thin film transistor (TFT)	0.225	Piezoelectronic	254	[18]
ZnO thin film	TFT			8.5	[37]
Li-doped ZnO thin film	TFT		Piezoelectronic	85	[16]
ZnO NW	Strain-gated transistor	2.1 uS	Piezoelectronic	233	[12]
2D ZnO nanoplatelets	Transistor	7.82×10^{-2} meV	Piezoelectronic	12700	[15]
PDMS pyramids	Parallel plate capacitor	2.82×10^{-2} V	Triboelectric	63.5	[23]
PDMS micropyramids	Parallel plate capacitor	0.2	Capacitive	165	[22]
Au NWs-impregnated tissue paper	Resistive	1.14	Resistive	5.1	[19]
ZnO NWs	Schottky diode		Piezo-phototronic	254	[11]
ZnO NT	**Schottky diode**	**1.95×10^{-3}**	**Piezoelectronic**	**1058**	**This work**
Human Skin				508	[2]

seen for the device composed of ZnO NTs with diameters of 500 nm.

The free-standing addressable devices were supported by the PI layer, which provided flexibility for bending and twisting (as shown in Fig. S10). To understand the device performance during bending, device AD20 was bent under two different bending conditions, and the pressure responses from the different pixels were measured. Fig. S11a–g shows the pressure responses of different diagonal pixels and compares the effects of different bending conditions. We observed no considerable change in the pressure response upon bending. Therefore, the device performance and the spatial resolution were also expected to be unaltered. Interestingly, the electrical contacts were strong enough to tolerate bending of the substrates, which indicated the good flexibility and robustness of the devices. Mechanically strong, flexible, and conducting graphene layers on the bottom of the ZnO NTs played a vital role in maintaining electrically stable electrodes. The conformal coating of the top contact and graphene on the bottom contact improved the robustness of the devices.

However, we prepared two-terminal piezoelectric sensor arrays with very high resolution by utilizing these crossbar array electrode nanodevices. The spatial resolution was 635 dpi for the device with AD20 (pixel size: 20 × 20 μm^2; pitch: 40 μm), while it was 1058 dpi for the device with AD12 (pixel size: 12 × 12 μm^2; pitch: 24 μm). Table 1 shows a comparison of tactile sensors from earlier reports. We found that the spatial resolution in the present case was very high compared to those of earlier reports on two-terminal/three-terminal tactile sensor arrays with aligned 1D/2D nanostructures. A few reports described extremely high resolution for cases in which the sensor exhibited the combined effect of photonics and piezotronics[2,10,26–28]. Two-terminal 1D nanostructure-based high-resolution piezotronic tactile sensors have not yet been explored. However, fabrication of piezotronic tactile sensors composed of 1D nanostructures on flexible substrates with high spatial resolution and compact integration for scalable manufacturing has remained a substantial manufacturing challenge. A few flexible capacitive tactile sensors with high sensitivity and reliability have been developed[22,23]. Resolution is still a great challenge in capacitive tactile sensors. However, piezo-phototronic image sensors have been developed with enormous spatial resolution, rapid response times and device flexibility[2,10,13,26–28]. Our approach with additional engineering in material growth and device fabrication opens a new direction for the field of high-resolution and flexible piezotronic tactile sensors.

Spatial mapping of tactile pressure from the addressable devices

Spatial mapping of tactile pressure was also performed by using an AD20 device composed of ZnO NT arrays with diameters of 1 μm. Figure 5a shows a sche matic representation of the measurement setup (upper panel) and the corresponding digital photograph

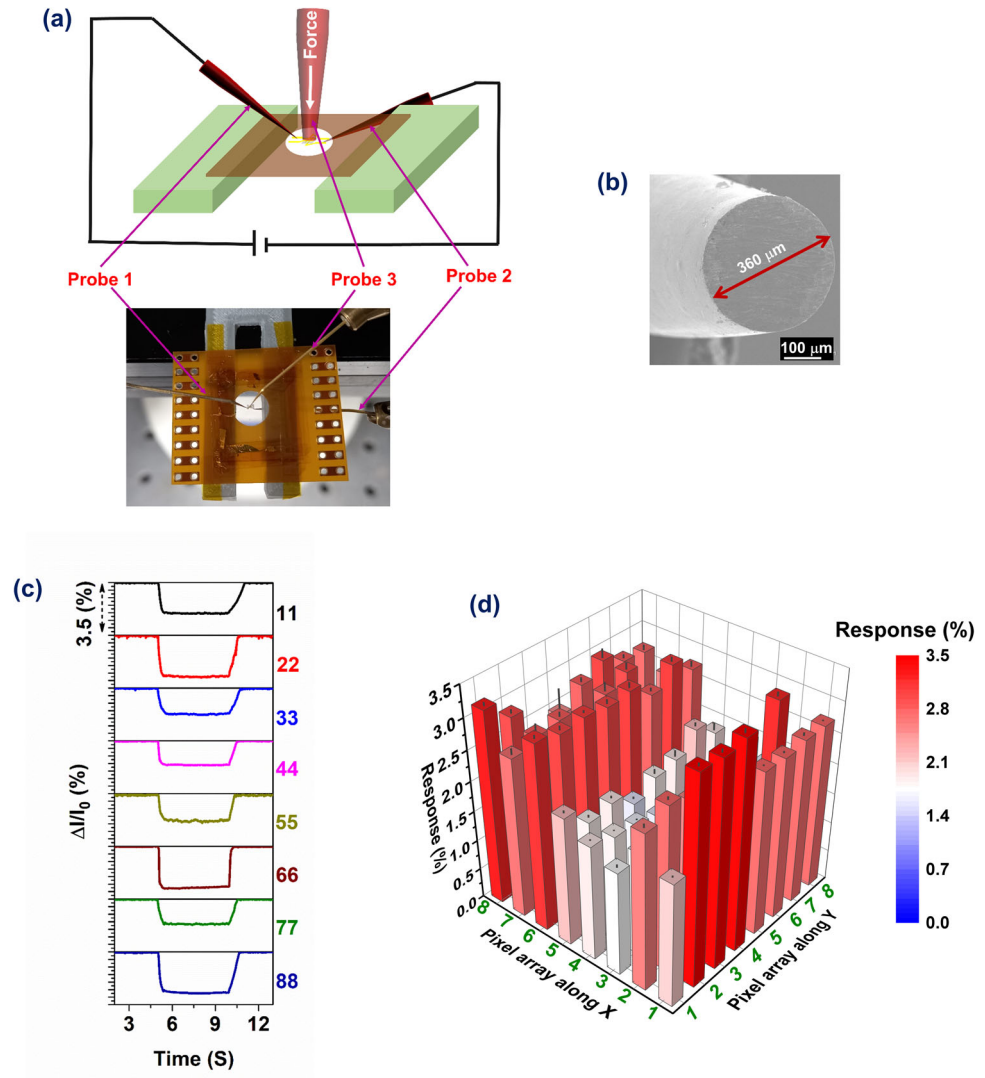

Fig. 5 Spatial distribution of the pressure responses at uniform mechanical pressure. a Schematic illustration of the experimental setup (upper panel) used for detection of tactile pressure. Corresponding digital photograph (bottom panel). **b** SEM image of the tip of the probe (3rd probe in **a**) with which pressure was applied. **c** Comparison of the *I–V* data from eight diagonal pixels in device AD20. **d** Corresponding real-time responses. **e** Spatial distribution of the pressure response from each addressable device in the 8 × 8 pixel array.

(bottom panel). A metal probe (3rd probe in Fig. 5a) om the flat surface was used to apply the vertical tactile force on the sample. Since the total device area was 300 × 300 μm^2, the tip of the probe had a size of 400 μm so that it covered the devices entirely (see Fig. 5b). Figure 5c, d shows the IV and IT data for different pixels. Figure 5e shows a spatial map of the pressure response. Each sensor in the pixel array felt the touch and responded efficiently; therefore, the sensors could be used as pixel-addressable devices. However, nonuniformities in response were observed; the probable reason is mentioned above. Additionally, the random responses could also originate from a nonuniform tactile force used to form an uneven surface.

Application of pixel-addressable device: image sensor

Pressure-resolved imaging was performed with an object to demonstrate a potential application of the tactile sensor array (see the SEM image in Fig. 6a). Significant responses were observed from the pixels in contact with the object. Figure 6b shows the IT of different pixels chosen from among the diagonally positioned pixels in the device. Figure 6c shows a spatial map of the pressure response imparted by the object. This observed non-uniformity should be improved by optimizing the growth and fabrication processes to obtain practical high-resolution sensor arrays. These devices may find application in electronic skins due to their high spatial resolution, flexibility, and wide pressure detection range.

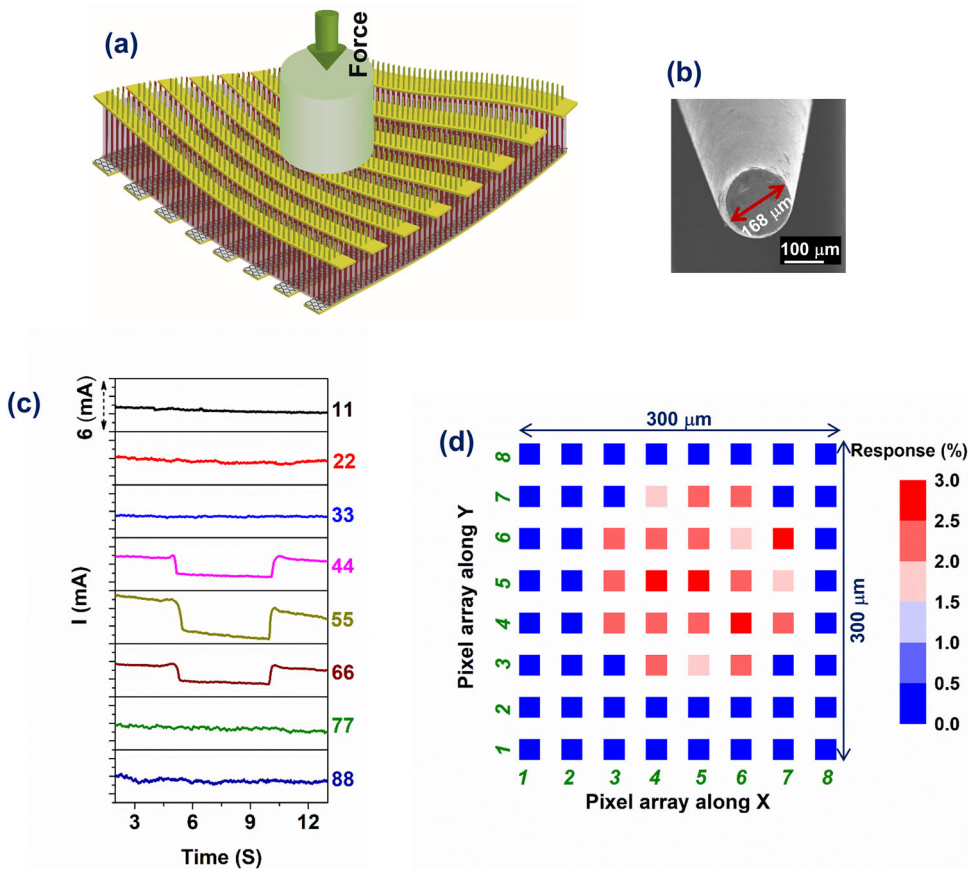

Fig. 6 Application of pixel-addressable device as image sensor. a Schematic illustration of pressure mapping. **b** SEM image for the tip of the probe used for pressure-resolved imaging. **c** Comparison of the real-time responses from eight diagonal pixels in device AD20. **d** Contour plot illustrating the capability of 8 × 8 addressable device arrays for imaging the spatial profile of applied stress.

Conclusions

In summary, individually addressable, high-density, dimension- and position-controlled, vertical, and free-standing piezoelectric sensor arrays were fabricated using ZnO nanotube arrays on CVD graphene layers. The individually addressable pixel matrix was fabricated by arranging the top and bottom electrodes of the sensors in a crossbar configuration. Furthermore, we revealed the uniformity and robustness in spatial mapping of pressure/force caused by the pixel size, the number of ZnO nanotubes in each pixel, and the lateral dimension of individual ZnO nanotubes by conducting a series of investigations. A spatial resolution as high as 1058 dpi was demonstrated for a Schottky diode-based tactile sensor composed of ZnO nanotubes on a flexible substrate. Additionally, we confirmed the excellent flexibility and electrical robustness of the free-standing sensor arrays for high-resolution tactile imaging. We believe that this work will attract much interest for 1D piezoelectric pressure/force sensor arrays with numerous potential applications in human-electronics interfaces, smart skin, and micro- and nanoelectromechanical systems.

Acknowledgements

We acknowledge the Brain Korea 21-Plus Program and Institute of Applied Physics, Seoul National University, for financial support to carry out part of this work. We further acknowledge Science Research Center (SRC) for Navel Epitaxial Quantum Architectures (NRF-2021R1A5A1032996). This work was also supported by the Samsung Research Funding Center of Samsung Electronics (SRFC-TA1803-02(0417-20180116)).

Author details

[1]Department of Physics and Astronomy & Institute of Applied Physics, Seoul National University, Seoul 08826, Republic of Korea. [2]James Watt School of Engineering, University of Glasgow, Glasgow G12 8QQ, UK. [3]Research Institute of Advanced Materials (RIAM), Seoul National University, Seoul 08826, Republic of Korea. [4]Department of Electrical and Computer Engineering, University of California San Diego, La Jolla, CA 92093, USA. [5]School of Advanced Materials Science and Engineering, Sungkyunkwan University, Suwon 16419, South Korea. [6]Department of Material Science and Engineering, Seoul National University, Seoul 08826, Republic of Korea

Author contributions

J.B.P.: Conceptualization, methodology, investigation, data curation. R.G.: Conceptualization, methodology, formal analysis, investigation, writing, review & editing. M.S.S.: Methodology & investigation. Y.H.: Investigation. Y.T.: Investigation. R.K.S.: Methodology & investigation. A.A.: Investigation. P.G.: Investigation. B.K.: Investigation & validation. S.-W.K.: Investigation & validation. M.K.: Investigation. G.-C.Y.: conceptualization, project administration, funding acquisition, formal analysis & investigation.

Conflict of interest
The authors declare no competing interests.

Publisher's note
Springer Nature remains neutral with regard to jurisdictional claims in published maps and institutional affiliations.

Supplementary information The online version contains supplementary material available at https://doi.org/10.1038/s41427-022-00386-4.

Received: 14 December 2021 Revised: 29 March 2022 Accepted: 1 April 2022.
Published online: 13 May 2022

References

1. Wang, Z. L. Progress in piezotronics and piezo-phototronics. *Adv. Mater.* **24**, 4632–4646 (2012).
2. Bao, R. et al. Flexible and controllable piezo-phototronic pressure mapping sensor matrix by ZnO NW/p-polymer LED array. *Adv. Funct. Mater.* **25**, 2884–2891 (2015).
3. Choi, M. Y. et al. Mechanically powered transparent flexible charge-generating nanodevices with piezoelectric ZnO nanorods. *Adv. Mater.* **21**, 2185 (2009).
4. Lee, K. Y., Gupta, M. K. & Kim, S. W. Transparent flexible stretchable piezoelectric and triboelectric nanogenerators for powering portable electronics. *Nano Energy* **14**, 139–160 (2015).
5. Oh, H. & Dayeh, S. A. Physics-based device models and progress review for active piezoelectric semiconductor devices. *Sensors* **20**, 3872–3909 (2020).
6. Ha, M. et al. Bioinspired interlocked and hierarchical design of ZnO nanowire arrays for static and dynamic pressure-sensitive electronic skins. *Adv. Funct. Mater.* **25**, 2841–2849 (2015).
7. Wang, Z. L. & Song, J. Piezoelectric nanogenerators based on zinc oxide nanowire arrays. *Science* **312**, 242–246 (2006).
8. Hu, W. G., Zhang, C. & Wang, Z. L. Recent progress in piezotronics and tribotronics. *Nanotechnology* **30**, 042001–042019 (2019).
9. Ghosh, R. et al. Fabrication of piezoresistive Si nanorod-based pressure sensor arrays: A promising candidate for portable breath monitoring devices. *Nano Energy* **80**, 105537 (2021).
10. Peng, Y. et al. Achieving high-resolution pressure mapping via flexible GaN/ZnO nanowire LEDs array by piezo-phototronic effect. *Nano Energy* **58**, 633–640 (2019).
11. Han, X., Du, W., Yu, R., Pan, C. & Wang, Z. L. Piezo-phototronic enhanced UV sensing based on a nanowire photodetector array. *Adv. Mater.* **27**, 7963–7969 (2015).
12. Wu, W. Z., Wen, X. N. & Wang, Z. L. Taxel-addressable matrix of vertical-nanowire piezotronic transistors for active and adaptive tactile imaging. *Science* **340**, 952–957 (2013).
13. Pyo, S., Lee, J., Bae, K., Sim, S. & Kim, J. Recent progress in flexible tactile sensors for human-interactive systems: from sensors to advanced applications. *Adv. Mater.* **33**, 2005902 (2021).
14. Wan, Y., Wang, Y. & Guo, C. F. Recent progresses on flexible tactile sensors. *Mater. Today Phys.* **1**, 61–73 (2017).
15. Liu, S. et al. Ultrasensitive 2D ZnO piezotronic transistor array for high resolution tactile imaging. *Adv. Mater.* **29**, 1606346 (2017).
16. Song, M. et al. Flexible Li-doped ZnO piezotronic transistor array for in-plane strain mapping. *Nano Energy* **55**, 341–347 (2019).
17. Chen, W. F. & Yan, X. Progress in achieving high-performance piezoresistive and capacitive flexible pressure sensors: a review. *J. Mater. Sci. Technol.* **43**, 175–188 (2020).
18. Oh, H., Yi, G.-C., Yip, M. & Dayeh, S. A. Scalable tactile sensor arrays on flexible substrates with high spatiotemporal resolution enabling slip and grip for closed-loop robotics. *Sci. Adv.* **6**, eabd7795 (2020).
19. Gong, S. et al. A wearable and highly sensitive pressure sensor with ultrathin gold nanowires. *Nat. Commun.* **5**, 3132 (2014).
20. Lee, J. H. et al. A behavior-learned cross-reactive sensor matrix for intelligent skin perception. *Adv. Mater.* **32**, 2000969 (2020).
21. Zhong, W. et al. Ultrasensitive wearable pressure sensors assembled by surface-patterned polyolefin elastomer nanofiber membrane interpenetrated with silver nanowires. *ACS Appl. Mater. Interfaces* **10**, 42706–42714 (2018).
22. Tee, B. C.-K. et al. Tunable flexible pressure sensors using microstructured elastomer geometries for intuitive electronics. *Adv. Funct. Mater.* **24**, 5427–5434 (2014).
23. Jiang, X.-Z., Sun, Y.-J., Fan, Z. & Zhang, T.-Y. Integrated flexible, waterproof, transparent, and self-powered tactile sensing panel. *ACS Nano* **10**, 7696–7704 (2016).
24. Yang, J. C. et al. Microstructured porous pyramid-based ultrahigh sensitive pressure sensor insensitive to strain and temperature. *ACS Appl. Mater. Interfaces* **11**, 19472–19480 (2019).
25. Tao, J. et al. Self-powered tactile sensor array systems based on the triboelectric effect. *Adv. Funct. Mater.* **29**, 1806379 (2019).
26. Pan, C. et al. High-resolution electroluminescent imaging of pressure distribution using a piezoelectric nanowire LED array. *Nat. Photonics* **7**, 752–758 (2013).
27. Li, X. et al. Enhancing light emission of ZnO-nanofilm/Si-micropillar heterostructure arrays by piezo-phototronic effect. *Adv. Mater.* **27**, 4447–4453 (2015).
28. Li, X. et al. Flexible light emission diode arrays made of transferred Si microwires-ZnO nanofilm with piezo-phototronic effect enhanced lighting. *ACS Nano* **11**, 3883–3889 (2017).
29. Tchoe, Y. et al. Individually addressable, high-density vertical nanotube Schottky diode crossbar array. *Nano Energy* **76**, 104955 (2020).
30. Lee, C.-H. et al. Flexible inorganic nanostructure light-emitting diodes fabricated on graphene films. *Adv. Mater.* **23**, 4614–4619 (2011).
31. Oh, H. et al. Vertical ZnO nanotube transistor on a graphene film for flexible inorganic electronics. *Small* **14**, 1800240 (2018).
32. Park, J. B. et al. Highly sensitive and flexible pressure sensors using position- and dimension-controlled ZnO nanotube arrays grown on graphene films. *Npg Asia Mater.* **13**, 57 (2021).
33. Papageorgiou, D. G., Kinloch, I. A. & Young, R. J. Mechanical properties of graphene and graphene-based nanocomposites. *Prog. Mater. Sci.* **90**, 75–127 (2017).
34. Nela, L., Tang, J., Cao, Q., Tulevski, G. & Han, S.-J. Large-area high-performance flexible pressure sensor with carbon nanotube active matrix for electronic skin. *Nano Lett.* **18**, 2054–−2059 (2018).
35. Kim, Y.-J. et al. Position- and morphology-controlled ZnO nanostructures grown on graphene layers. *Adv. Mater.* **24**, 5565–5569 (2012).
36. Smit, G. D. J., Rogge, S. & Klapwijk, T. M. Scaling of nano-Schottky-diodes. *Appl. Phys. Lett.* **81**, 3852–3854 (2002).
37. Vishniakou, S. et al. Tactile feedback display with spatial and temporal resolutions. *Sci. Rep.* **3**, 2521 (2013).